Determining Thorpe Scales from Ship-Lowered CTD Density Profiles

ANN GARGETT AND TERESA GARNER

Old Dominion University, Norfolk, Virginia

(Manuscript received 8 November 2006, in final form 18 December 2007)

ABSTRACT

CTD measurements taken as an integral part of oceanographic cruises could provide valuable information on spatial locations and time variability of significant shear-generated mixing in the ocean interior if used routinely to calculate Thorpe scales, that is, estimates of the scales of vertical overturning in an otherwise stably stratified fluid. This paper outlines methods for calculating reliable Thorpe scales from density profiles taken with a shipborne CTD, including removal of questionable instabilities associated with termination of pressure reversals, reduction of the effects of density noise by computation of an intermediate density profile, and overturn verification by a two-parameter (R_o, ΔN) diagnostic. The R_o criterion alone reliably removes overturns that result from salinity spikes at the high gradient boundaries of a weakly stratified layer, a common cause of highly suspect overturns. The ΔN diagnostic is a new water mass test describing the degree of "tightness" of the temperature–salinity (T–S) relationship. The present two-parameter diagnostic rejects a significantly larger percentage of suspect overturns than does a previous single-parameter water mass test. Despite developing a more reliable water mass diagnostic, the authors conclude that rejection of overturns based on a water mass test that incorporates expectation of T–S tightness is not warranted, given possibilities of T–S "looseness" resulting from mixing over regions of nonlinear T–S structure and/or from potential effects of differential diffusion.

1. Introduction

Over the past few decades, the workhorses of ocean turbulence measurement have been freefall profilers measuring temperature and/or velocity microstructure, small-scale fluctuations widely presumed to be generated in deep ocean environments primarily by shear instabilities associated with the ocean internal wave field. Such profilers provide accurate measurements of the dissipation scales of ocean turbulence, but because of their complexity and cost they have operated only in limited areas for limited periods of time. To address the resulting paucity of ocean turbulence data, Naveira Garabato et al. (2004) recently suggested the use of data routinely collected by standard hull-mounted ADCPs operated on oceanographic transects. The purpose of the present paper is to suggest that reliable estimates of another turbulence parameter, the Thorpe scale L_T, can be made using another accessible and familiar piece of equipment operated routinely on oceanographic cruises, a wire-lowered CTD. Thorpe (1977) originally proposed a stable sort method to estimate vertical overturning scales of the large eddies associated with shear-generated turbulence in stably stratified water columns. Although we are accustomed to thinking of ocean turbulence measurements as those of dissipation scales, that is to a large extent because these are the scales measured by microscale profilers, not because they are inherently the most important turbulent scales *to* measure. Indeed, it could be argued that the energy-containing scales are more important, both because they provide fundamental evidence of the processes connecting external forcing of three-dimensional turbulence and turbulent dissipation scales and because they are important to various applications (e.g., assessing the effects of varying ambient light intensity on phytoplankton productivity). In fact, a common use of microscale measurements of turbulent kinetic energy dissipation rate ε is to *predict* the vertical scale of the largest eddies via the buoyancy length scale $L_o = (\varepsilon/N^3)^{1/2}$, a relationship (Dougherty 1961) among vertical length scale, dissipation rate of turbulent kinetic energy per unit mass ε, and background density stratifica-

Corresponding author address: Ann Gargett, Center for Coastal Physical Oceanography, Old Dominion University, Norfolk, VA 23508.
E-mail: gargett@ccpo.odu.edu

DOI: 10.1175/2008JTECHO541.1

tion [characterized by buoyancy frequency $N = (-g\rho_o^{-1}\rho_z)^{1/2}$ calculated from the vertical density gradient ρ_z]. Widespread distribution of shipborne CTD profiles in space and time thus offers an opportunity to derive global maps, like those routinely produced for temperature (T), salinity (S), and other water properties, for a turbulent quantity of major relevance.

Thorpe (1977) argued that a gravitationally unstable region in an otherwise stably stratified fluid can be only a transient condition, created as a large eddy of a three-dimensional turbulent field temporarily overturns density surfaces. "Large" is used here in a relative sense, referring to the largest scale of three-dimensional motions that deliver energy directly to a turbulent cascade, hence irreversibly to dissipation scales (Tennekes and Lumley 1972). The appearance of inversions in a vertical density profile is therefore a strong indicator of the presence of turbulent mixing. To quantify the vertical overturning scale associated with the large eddies of turbulence, Thorpe (1977) sorted temperature profiles observed in a freshwater loch to a stable state, keeping track of the minimum vertical distance each parcel of water had to be moved to establish the stable condition. The Thorpe displacement assigned to depth d_i is $L_t(d_i) = d_f - d_i$, where d_f is the depth to which the point originally at d_i has been moved: thus, positive (negative) Thorpe displacements correspond to downward (upward) relocation of a water parcel. The Thorpe length scale L_T is the root-mean-square of all Thorpe displacements within a complete overturn, defined as a vertical distance over which Thorpe displacements sum to zero.

Thorpe (1977) sorted temperature, a property that is the sole determinant of density in freshwater systems and easy to resolve on the scales of tens of centimeters and larger at which significant overturns occur [Stansfield et al. (2001) showed that although small Thorpe displacements are more probable than large ones, it is the latter, more easily measurable ones, that dominate L_T]. Although T profiles have been used to calculate L_T in some oceanic regions and/or over restricted depth horizons (Alford and Pinkel 2000), temperature does not everywhere dominate the density of oceanic waters. In subpolar and polar oceans as well as in coastal and frontal regions, S contributes to and may dominate seawater density σ_t.[1] Problems associated with the determination of S from measurements of T, conductivity C, and pressure p propagate into the calculated density, resulting in density profiles with higher random and systematic noise levels than T profiles. Nevertheless, if we seek a uniform global application, oceanic Thorpe scales must be calculated by sorting density rather than temperature.

Although the underlying idea is straightforward, the accuracy of Thorpe scale estimates depends on all possible sources of error associated with data collection and interpretation. In estimating reliable Thorpe scales from density profiles derived from shipborne CTD data, one set of issues (discussed in section 2) is specific to the ship as platform: (i) translation of ship motions into variability of the lowering rate of the CTD package and (ii) possible contamination of near-surface measurements by wash from propellers and/or thrusters and interaction of surface waves with the hull. Other issues are associated with familiar errors inherent to the CTD measurement of density: effects of (iii) sensor noise levels and (iv) temperature and conductivity sensor responses. The error associated with sorting density values that contain errors is not readily quantified, as error in averaging those same values is quantified by their standard deviation. Thus, it is essential to process CTD data before sorting in ways that minimize both types of erroneous data; methods for optimizing calculation of density from standard CTD data are reviewed in section 3. Section 4a outlines a method of minimizing effects of random density noise in the sorted profile. In section 4b, a two-parameter test is designed to reject false overturns associated with possible residual effects of imperfect sensor matching, and results are compared with a water mass test devised by Galbraith and Kelley (1996, henceforth GK96). The desirability of actually implementing such a water mass test is reconsidered in this section. Section 5 illustrates the use of Thorpe scale measurements and discusses their potential as a survey tool for the spatial and temporal exploration of sites of shear-generated turbulent mixing in the ocean.

The data used in this study were taken with Sea-Bird Electronics SBE9*plus* CTDs, operated from the R/V *Nathaniel B. Palmer* (*NBP*) during two Mixing and Ultraviolet Radiation in the Ross Sea (MIXURS) cruises in austral summer 2004/05 (cruise identifier 409) and austral spring 2005 (cruise identifier 508). Records are designated as CCCsss_Di, where CCC is the three-digit cruise identifier, sss is the session number (a session is a set of consecutive downcasts) and i is the cast number within a session. Although much of this data was taken in weak to moderate wind and sea states within the Ross Sea, several CTD sessions there took place in open water during conditions marginal for CTD operation. We also use two available open ocean stations taken during transit between the Ross Sea and New

[1] Density is represented by σ_t, the value of $\sigma = \rho - 1000\ \mathrm{kg\ m^{-3}}$ referenced to the surface, a definition which is adequate for the shallow profiles considered here. For deeper measurements, the pressure reference level should be increased appropriately.

Zealand, one (58°6.78′S, 178°11.56′E) within the Antarctic Circumpolar Current and one (47°3.1′S, 174°15.96′E) in the South Pacific subtropical gyre. The dataset thus contains the full range of sea state conditions in which shipboard CTD operation is possible. The typically weakly salt-stratified polar water columns that furnish most of our data also provide the most extreme challenge for CTD density measurements.

2. Ship effects

CTD scans of T, C, and p are recorded at even increments of time, so if lowering speed $F > 0$ is constant, time (t) and depth (d) are simply related by $d = Ft = Fs_i\delta t$, where s_i is the scan number, F is the fall speed, and δt is the time interval between scans. However, fall speed variation due to the effect of ship motion on the hard-coupled CTD can be substantial; indeed, ship heave motion may be so large that F occasionally reverses sign for short periods. Thus, the first steps in processing shipborne CTD profiles locate sections of pressure reversals and edit out data between successive encounters of the same pressure. The resulting pressure-edited property series may be viewed as functions either of the edited scan number s_i^e, an index made by renumbering the original scans after pressure editing, or of the pressure associated with the remaining samples. The series that result from pressure editing have equal spacing in s_i^e but unequal spacing in pressure if F varies through a profile. Thus, a fundamental choice when calculating L_T is whether to sort scan-based or pressure-based property profiles. Previously published results use the recorded pressure time series to interpolate scans to regular spacing in pressure before sorting the resulting pressure-based time series. Although variability in pressure and depth sampling (apparently) disappears in the interpolated series, aliasing due to inadequate spatial sampling may nonetheless be present in the resulting property profiles. An alternate procedure is to sort the scan(time)-based series to produce Thorpe index displacements L_t^i and, subsequently, convert these to distance by multiplying by a local fall speed; thus, $L_t = \overline{F}L_t^i$, where $\overline{F}$ is the fall speed averaged over the extent of an overturn.

There is no uncertainty associated with the sort variable in the scan-sort technique, as there is if the sort variable (i.e., pressure) is itself a measured quantity. Error in the resulting Thorpe scale is associated with uncertainty in the fall speed (used to convert from scan index to vertical distance) over the vertical extent of an identified overturn, and this uncertainty is readily quantified. Examples of fall speed variation over the range of sea states encountered are seen in Fig. 1. The

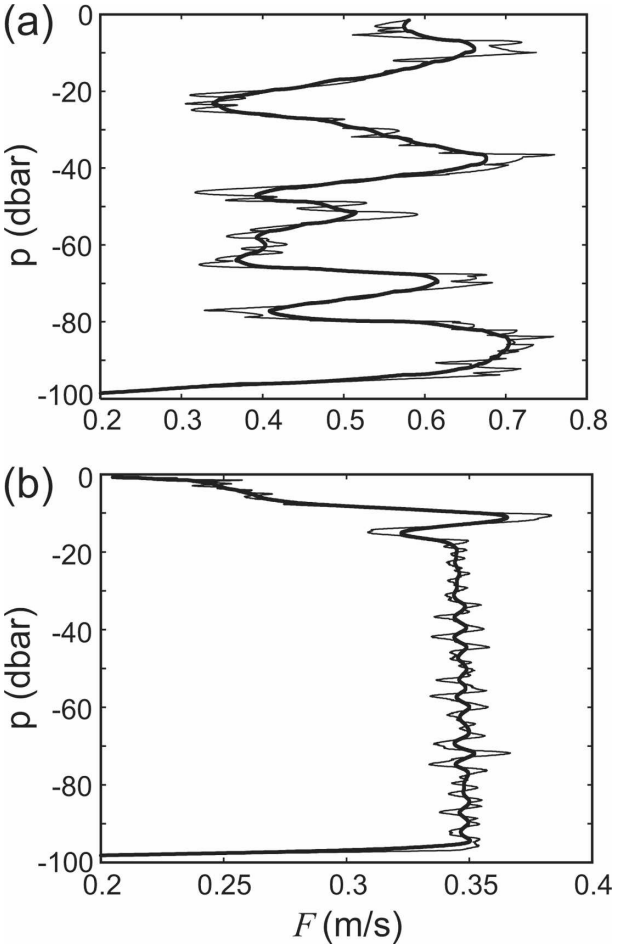

FIG. 1. Raw fall speed (thin line), calculated by differencing edited filtered pressure over a vertical distance of approximately 3 m, and a smoothed version (heavy line) used to convert Thorpe index displacements to vertical distance. (a) Profile 409074_D1, taken just before CTD operations were suspended due to weather conditions and (b) profile 409161_D1, taken in nearly flat calm conditions, illustrate the range in fall speed variability.

thin line is "instantaneous" fall speed F_i (calculated from low-pass-filtered pressure differenced over ~3 m); F_o (thick line) is a smoothed version. For a CTD cast taken just before operations were suspended due to the high sea state (Fig. 1a), the maximum percentage error over nine identified overturns is 11% (15%) in smoothed (raw) fall speed. Mean errors for the nine overturns are considerably lower, respectively, 6% and 9%; hence, most overturns have smaller errors. For benign conditions (Fig. 1b; note change of scale), differences are much smaller: mean errors are only 0.3% (0.9%) for smoothed (raw) fall speed.

Although the procedure of removing pressure reversals due to ship heave is straightforward, it has the potential to generate false density overturns. As a result

of combined ship motion and horizontal water property gradients, the CTD may encounter a slightly different water mass when it returns to a previously sampled depth.[2] Figure 2 shows density differences between consecutive encounters of a pressure value as a function of the time extent of the pressure reversal for two profiles that span the observed range of sea state. To avoid possible identification of false overturns in pressure-edited measurements, unstable density values immediately below data gaps ($\delta\sigma_t < 0$ in Fig. 2) are replaced by interpolated (stable) values.

Shipborne operation also makes it impossible to make uncontaminated near-surface measurements of turbulence properties. It is obvious that turbulence generated by the hull contaminates water property profiles above the depth of the ship's draft (here ~6.4 m). However, intermittent ship-generated turbulence on the *NBP* could occasionally be observed at depths 3–4 times the draft, appearing as abnormally noisy near-surface CTD data (identified by comparisons within a profile and/or between profiles within a session; not shown) and/or very high backscatter in the hull-mounted echo sounder record, attributed to bubble clouds generated by the operation of propellers and the bow thruster (an example will be seen in a later figure). In general, the fact that ship-generated turbulence may extend to depths considerably greater than hull depth must be considered when selecting a minimum depth for calculating Thorpe scales.

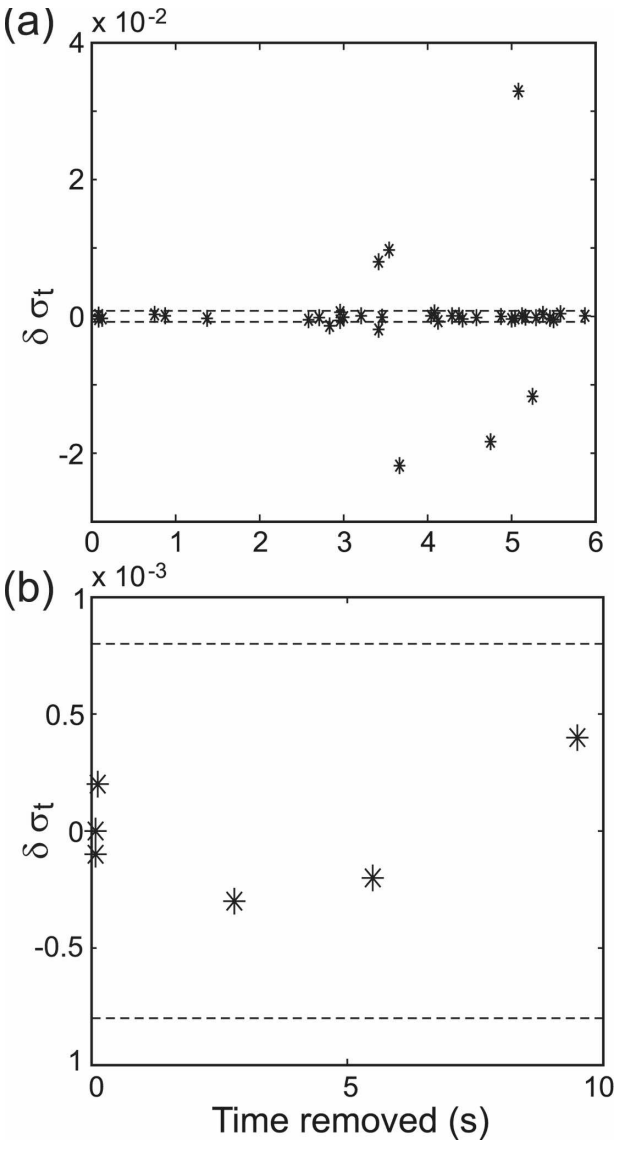

FIG. 2. Values of $\delta\sigma_t$, the difference of σ_t values encountered at the beginning and end of a period of reversed pressure, as a function of the amount of time removed: (a) 409074_D1, a record where 42.9% has been removed, and (b) 409161_D1, a record where the 5.6% removed is all at either the start or end of the cast. Note scale changes between the two. Horizontal lines indicate the threshold value (0.0008 kg m^{-3}) used to define density changes above noise for cruise NBP409 (see section 4). All densities within unstable ($\delta\sigma_t < 0$) regions are replaced by values interpolated between the point immediately above the pressure reversal and the first stable point following it, removing the possibility of false overturns generated by vessel heave.

3. Optimizing calculation of density

In addition to the platform effects discussed above, various sensor issues influence determination of Thorpe scales. Because the SBE9*plus* has become the de facto standard on most large oceanographic vessels, its sensor response characteristics have been extensively studied. In particular, Sea-Bird processing software (Sea-Bird Electronics 2006) offers routines for minimizing salinity spiking and thermal lag.

Thermal lag, a consequence of the capacity of the conductivity sensor body to store heat, can lead to substantial differences of derived salinity between downcasts and upcasts, including large-scale (tens of meters) salinity (density) inversions within pycnoclines. Lueck and Picklo (1990) derived a conductivity correction that is a recursive filter defined by two variables: α, the initial amplitude of temperature change for a unit step change in ambient temperature and τ, the *e*-folding time of the temperature error. We use standard values of $\alpha = 0.03$ and $\tau = 7$ s as recommended in the Sea-Bird manual (Sea-Bird Electronics 2006) for the SBE9*plus* pumped at 30 cm^3 s^{-1} (0.030 L s^{-1}).

[2] A reviewer pointed out that because most CTDs are deployed on Rosette samplers, large heave motions might also result in the CTD sampling water that had been entrained and mixed within the Rosette during a pressure reversal.

Salinity spikes, familiar artifacts arising from mismatches between time responses of the C and T sensors, propagate into the calculation of density where they can lead to false density inversions. Zero-order sensor lag, calculated from the C-cell pumping rate and the spatial separation of the T and C sensors, was removed on acquisition. However, although Sea-Bird processing software offers the opportunity to further low-pass filter either conductivity or temperature and to shift C relative to T (in either direction) before calculating S and σ_t, no standard settings are offered for filter cutoff, number of seconds to shift, or which variable to shift (Sea-Bird Electronics 2006, 56–58, 69–71). Thus, salinity spiking was further reduced in our data (although never entirely eliminated) by an iterative program (after Morison et al. 1994) developed to identify, filter, and shift the output of the faster responding sensor before calculation of salinity. Because the alignment correction is not optimal for all spikes, we further reduced transmission of S spikes to density by a final low-pass filter with time constant 0.1 s. Temperature is run through this same filter to produce variables with consistent space–time resolution for use in the calculation of density. With a winch payout rate of $F \approx 30$ cm s^{-1} ($\sim$20 m min^{-1}, a typical "slow" CTD lowering rate), the SBE9*plus* 24-Hz sample rate provides raw samples with average vertical spacing of $\sim$1.3 cm. This resolution is reduced to $\sim$13 cm by the final low-pass filter.

4. Overturn validation

Even when optimal corrections have been made, CTD-derived density still contains random noise and residual effects of salinity spiking. This section describes methods to identify and reject potentially false overturns associated with these effects.

a. Treatment of random noise

Because random noise in density within a completely well-mixed region will lead to some parcels being sorted over nearly the full extent of the region, and hence to identification of an overturning scale equal in vertical extent to that of the well-mixed region, it is essential to find a means of identifying and rejecting false overturns associated with the presence of noise in regions of weak mean density gradient.

Thorpe (1977) required that the difference between data values at the same depth in the original and sorted T profiles be greater than the T noise: although effective, this method may underestimate the magnitude of true inversions by rejecting valid displacements within an overturning region, consequently lowering the value of the rms displacement for the patch. An alternate treatment of the noise problem, proposed by GK96, is based on lengths of runs, that is, groups of successive data values "running" in the same direction (either increasing or decreasing) within a time series. White noise typically contains many runs of short length and has a well-defined run length probability distribution function (PDF). GK96 compared the run length PDF of white noise with run length PDFs of σ_t within overturns and determined an empirical threshold that rms run length had to exceed for the inversion to be accepted as real. However, when Johnson and Garrett (2004) added uncorrelated random noise to a linear gradient of σ_t, they found that rms run lengths could be either greater or less than that expected for a random uncorrelated series with constant mean value, leaving the GK96 noise algorithm in some doubt. Piera et al. (2002) used wavelet techniques with various assumed noise thresholds to de-noise artificial density profiles, but they tested the resulting procedures only with measured temperature profiles.

We use instead a modified version of a profile preprocessing method (Ferron et al. 1998) that seeks to prevent noise-related overturns by creating an intermediate density profile that tracks only significant density differences in the original profile, a "significant" difference being defined as one greater than a threshold value related to the noise standard deviation of density. An intermediate profile is built by vertically traversing the original profile from top to bottom (i.e., down), copying its values directly to the intermediate profile as long as successive data values differ from each other by more than the threshold value. Differences less than the threshold value are excluded by retaining the preceding original data value in the intermediate profile; that is, the intermediate profile remains at a constant density until a density change greater than the threshold value occurs. Determination of the threshold value is based on the magnitude of random noise levels in σ_t. Because in situ noise levels may exceed manufacturer statements for a variety of reasons, a preferable method of noise determination uses actual cruise profiles, defining a property noise level as the standard deviation of values within a layer that is well mixed in the property. Noise levels determined in this manner for both raw and (our) processed density data from the SBE9*plus* used during NBP508 are shown in Table 1. Individual values result from different choices of "well mixed" layers within the cruise dataset. The threshold level is set as a multiple of the rms noise level. Increasing the multiple decreases the number of resulting overturns, rapidly at first as "typical" noise is no longer

TABLE 1. The rms noise level δ_D in both raw and processed σ_t from a selection of well-mixed layers during NBP508.

Record	Raw	Processed
	δ_D (kg m^{-3})	
P508060_D1	0.000 26	0.000 09
P508012_D1	0.000 27	0.000 08
P508104_D1	0.000 26	0.000 10
P508104_D4	0.000 30	0.000 16
P508119_D2	0.000 25	0.000 08
P508130_D2	0.000 28	0.000 12
Mean	0.000 27	0.000 10

sorted. Once the multiple reaches 4–5, further increase makes little change to the number of overturns identified (although there may be minor changes in overturn size). A multiple of 5 results in a density threshold level of 0.0005 kg m^{-3} for NBP508 (the equivalent level for NBP409 was somewhat higher, 0.0008 kg m^{-3}, as a result of higher noise in the temperature sensor).

Because an intermediate profile calculated by the method described above is influenced by the initial starting value (either the first value recorded or the first value deeper than some depth of ship influence), a second intermediate profile is calculated from the bottom to the top (i.e., up). While the "down" profile tracks a steep pycnocline from below (red profile, Fig. 3), the "up" profile (green profile, Fig. 3) tracks the same pycnocline from above, so their average (blue in Fig. 3) follows the actual profile more closely than either of the individual intermediate profiles. Thorpe displacements are calculated by sorting the average intermediate density profile.[3] To further decrease the sensitivity of the results to the initial values used to generate the down and up profiles, an identified overturn is retained only if (i) both profiles contain unstable density gradients and (ii) at least one unstable density gradient within the overturn is pressure coincident (within 0.1 dbar) in both profiles. The overturn seen in Fig. 3 is an example of one that passes the first but fails the second of these requirements.

A complete overturn, defined as a region within which scan-based Thorpe displacements sum to zero (the existence of which is ensured by the nature of the sort operation), must be identified to calculate the rms Thorpe scale. Because of ship-induced problems with near-surface data, discussed in section 2, the summation process that defines overturns is started at the bottom of a cast and proceeds upward. For the present data, an overturn that does not close below 10 m is discarded, so the processing underestimates near-surface overturns.

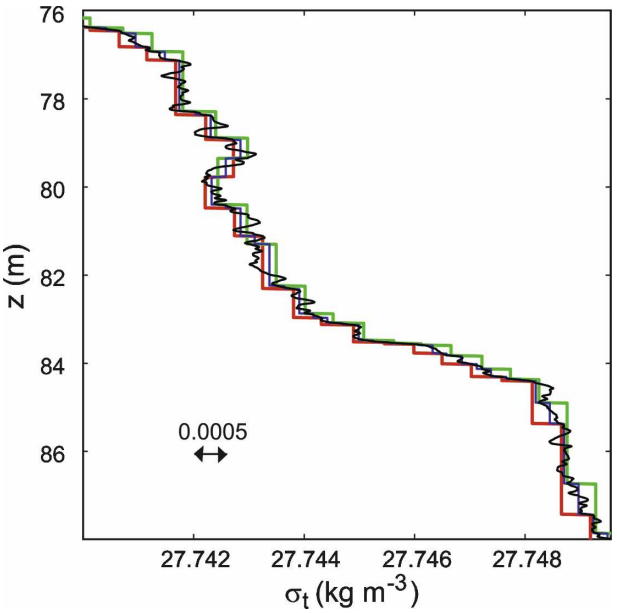

FIG. 3. Sample section of intermediate profiles generated from the top (down profile; red) and from the bottom (up profile; green) of a measured density profile (black). Each intermediate profile changes value only where the difference between successive measured density values exceeds a threshold related to density noise. Thorpe displacements are determined by sorting the average (blue) of down and up profiles to stability.

b. *Treatment of residual effects of sensor response*

The final stage of overturn validation seeks to ensure that false density overturns caused by inevitable residual sensor effects are identified and rejected with reasonable certainty, even at the cost of rejecting some actual overturns. Various methods of overturn validation have been used by previous authors. Some (e.g., Alford and Pinkel 2000) restrict attention to parts of the water column where T has a monotonic mean profile and accept density overturns only when these co-occur with T overturns, a technique that has obvious shortcomings for global application. A more elaborate diagnostic for rejection of false overturns in density caused by conductivity–temperature (C–T) response errors was devised by GK96 based on a specific expectation of the nature of the T–S relationship within an overturning region. GK96 argued that turbulent mixing within a region of locally linear T and S gradients does not change T–S characteristics; hence, all parcels within an overturn, however interchanged vertically and

[3] Note that the down and up profiles individually have a minimum density step that equals the chosen threshold value but their average, the profile that is finally sorted to stability, may have smaller minimum step size as a result of the averaging.

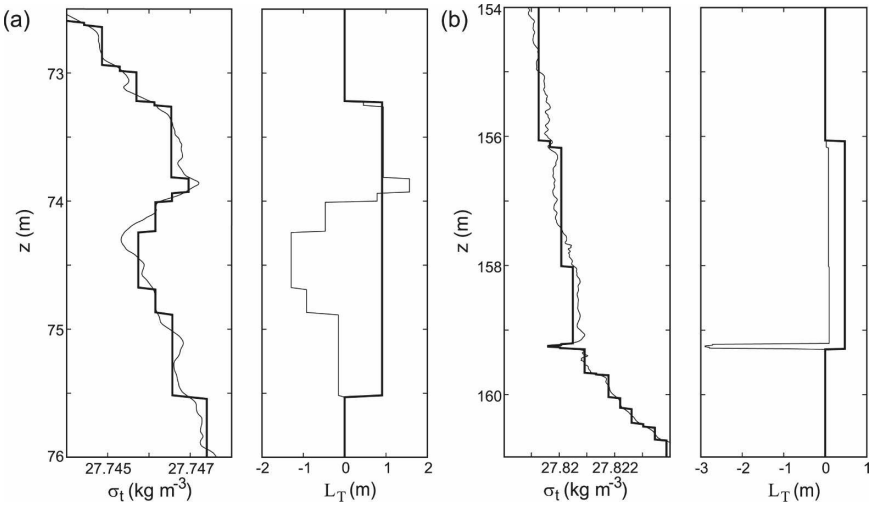

FIG. 4. (a) This overturn (point A in Figs. 7 and 8) approximates a classic S-shaped overturn, characterized by roughly equal distribution of positive and negative Thorpe displacements: $R_o = 0.34$. (right) Profile of filtered (light line) and intermediate (heavy line) density; (left) Thorpe displacement (light line) and root-mean-square Thorpe scale (heavy line). (b) A case (point B in Figs. 7 and 8) where remnants of a likely salinity spike at the base of an otherwise weakly stratified region produce a suspect overturn: $R_o = 0.02$. Right and left as in (a).

mixed or unmixed, should lie along the local *T*–*S* relationship. Imperfect *S* measurement due to *C*–*T* sensor response mismatch will cause deviations, identified by GK96 as "loops" off the locally linear *T*–*S* relationship. To characterize the nature of the observed *T*–*S* relationship, GK96 calculated two ratios, ξ_S and ξ_T,[4] and defined the diagnostic $\xi = \max(\xi_S, \xi_T)$. They argued that values of ξ near zero indicate a tight *T*–*S* relationship and large values signify a loose relationship, and quantified "large" by comparison with a visual score of the "tightness" of *T*–*S* relationships. Their visual inspection awarded each overturn a score between zero and one, with scores less than 0.5 assigned to overturns ". . . that would be discarded by the usual visual method of rejecting regions with loops in the T/S diagram." Correlation between visual scores and ξ values suggested that overturns with $\xi < 0.5$ could be accepted as true overturns.

As will be demonstrated shortly, the GK96 method did not provide clear identification of suspect overturns in our Southern Ocean data. Consequently, we developed an alternate method based on a pair of diagnostics calculated after overturning regions are defined in the Thorpe scale processing. The first is an overturn ratio, $R_o = \min(L^+/L, L^-/L)$, where L^+ and L^- are, respectively, the vertical distances occupied by positive and negative Thorpe displacements within an overturn of vertical extent *L*. A single perfect overturn sampled straight through the middle would contain equal lengths of positive and negative displacements, hence $R_o = 0.5$. A more complex and/or imperfectly sampled overturn would have R_o less than 0.5: the example shown in Fig. 4a has $R_o = 0.34$. In contrast, a low-density spike appearing at the base of a weakly stratified layer results in a small number of (large) negative displacements, as the points within the spike are sorted to the top of the layer, accompanied by a large number of (small) positive displacements as all the remaining points shift down slightly to accommodate them. Such situations are characterized by low values of R_o: the example seen in Fig. 4b has $R_o = 0.02$. From visual inspection of a large number of profiles, it was found that density overturns that would be declared suspect as a result of residual salinity spiking at large *C*–*T* gradients bracketing relatively well-mixed layers are associated with values of $R_o < 0.2$.

To address *C*–*T* sensor effects in more complex overturns, we also examined data in the *T*–*S* plane, following the suggestion of GK96 that *T*–*S* points within a reliably measured overturn should lie closely along the local *T*–*S* relation. Instead of working separately with *T* and *S*, as do GK96, we use an alternate measure of *T*–*S* tightness. First, given measurement uncertainty in both

[4] Taking ξ_S as an example, differences between observed σ_t and an estimate of σ_t based on a linear least squares fit to a σ_t –*S* relationship are calculated for all points within an individual overturning region. The ratio ξ_S is the rms value of these differences, normalized by the rms value of the Thorpe fluctuation density (observed minus sorted σ_t).

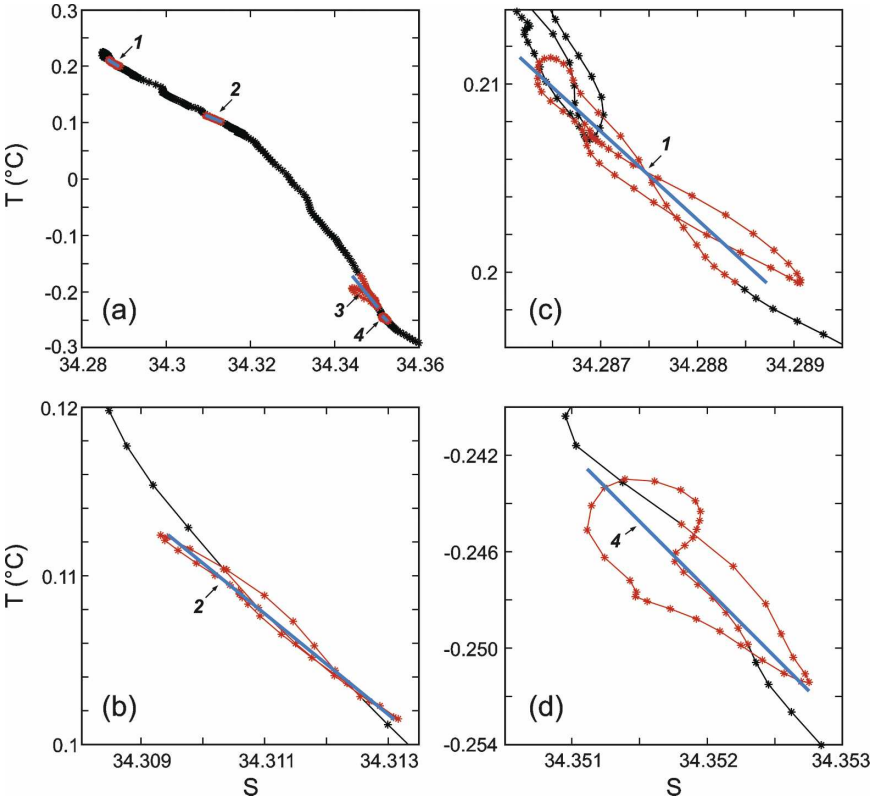

FIG. 5. Examples of the dependence of the visual impression of T–S tightness on resolution. (a) At this resolution only overturn 3 would be considered to have a loose T–S relationship. (b) Under increased resolution, overturn 2 retains a tight T–S relationship, but overturns 1c and 4d become loose.

T and S, we use the geometric mean of the slopes of two linear regressions (T on S and S on T; Ricker 1973) to define a best-fit T–S slope. If θ is the angle between this linear regression line and the S axis, measured data values (x, y) in coordinates oriented, respectively, along and normal to the local T–S relationship are given by

$$x = S\cos\theta + T\sin\theta \quad \text{and} \tag{1}$$

$$y = -S\sin\theta + T\cos\theta, \tag{2}$$

and the tightness of the T–S fit can be quantified either by normal variance, defined as

$$\sigma_n = \sqrt{\left(\frac{1}{M}\sum_{i=1}^{M} y_i\right)^2}, \tag{3}$$

or normal range

$$\Delta n = y_M - y_m, \tag{4}$$

where y_M and y_m are the largest positive and negative deviations of T–S points in the direction normal to the mean T–S line over the M points within an overturn. In the following discussions we use Δn, but similar results are found for σ_n. At this point, Δn is normal to the local T–S relationship. However, the importance of such variation depends upon the orientation of the local T–S relationship to local isopycnals, because only the component of the variation *normal to isopycnals* will lead to false overturns. Thus, our final diagnostic ΔN is the projection of Δn onto the direction normal to local isopycnals, a relative measure not only of how well data points inside an overturn follow a local (linear) T–S relationship but also of the importance of any deviations to the production of false density overturns.

To calibrate ΔN, we (like GK96) use visual inspection to determine a bounding value ΔN_o such that $\Delta N < \Delta N_o$ defines an acceptable degree of variability in the T–S relationship. A major difficulty is that T–S tightness of measured data depends on the degree of resolution with which the T–S plot is viewed, as illustrated in Fig. 5. With the scaling used in Fig. 5a, one might decide that overturn 3 has an unsatisfactory degree of T–S looping, but the remaining overturns are tight. However, with the exception of overturn 2 (Fig. 5b), all the overturns shown in Fig. 5a will appear loose if ex-

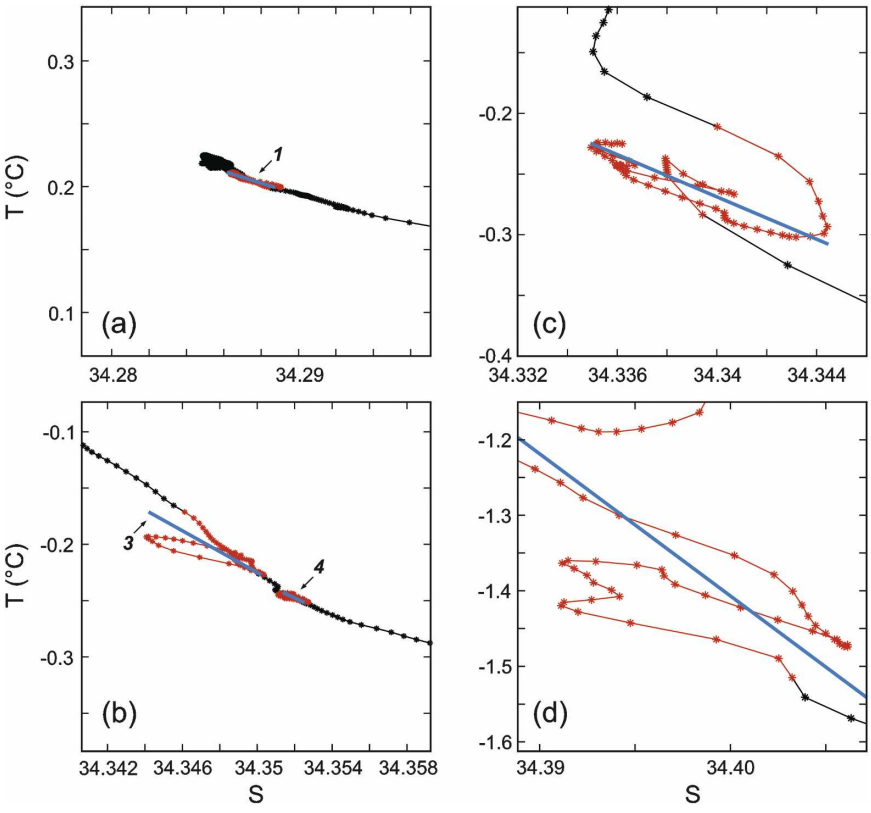

FIG. 6. Measured T–S points viewed in windows scaled to fixed density increment. Local T–S relationships (straight lines) are determined by linear least squares fit to the data points within individual overturns (red). (a) and (b) Overturns originally displayed in Fig. 8a. With this degree of resolution, overturn 1 and overturn 4 in (b) show tight T–S relationships and are qualified as good. Overturn 3 (point C in Figs. 7 and 8) has a resolved loop off the local T–S slope and is qualified as bad. (c) An example of an overturn classified as borderline because most of the T–S points within the overturn are parallel to the T–S curve below the overturn. (d) Part of a bad overturn (point D in Figs. 7 and 8) that exhibits a very loose T–S relationship (fixed window size precludes viewing the entire overturn).

amined with sufficient resolution (Figs. 5c,d). When making qualitative decisions about acceptable or unacceptable degrees of T–S variability in measurements, this visual relativity is a major issue, one not clearly addressed by GK96. Visual relativity is minimized in our qualitative decisions by using a fixed size for the smallest T–S window within which any portion of a T–S curve may be viewed. The size of the window in S is set as $\delta S = \Delta\rho/\beta\rho_o$, where $\beta(T, S, p)$ is the coefficient of haline contraction of seawater and $\Delta\rho$ is a density increment. The associated window dimension for T is then $\delta T = \beta\,\delta S/\alpha$, where $\alpha(T, S, p)$ is the coefficient of thermal expansion of seawater: both α and β are calculated with the central values of T and S from the selected overturn. The size of the resulting window corresponds to T and S ranges that produce equal density increments (given a locally linear equation of state). Fixing the size of the T–S window in (equivalent) density scales for the fact that the degree of density variability associated with S and/or T variability depends upon the degree to which each property affects seawater density, a degree that can change dramatically between particular locales and/or depths. For example, where S dominates density (as in our high-latitude Ross Sea measurements), S variation about the local T–S relationship is important, but T variation is much less significant. In such regions, $\beta/\alpha \approx 20$ is considerably larger than values (typically ~3) in subtropical and equatorial regions. Thus, for the same δS, δT is larger in subpolar than in subtropical regions, visually compressing the (relatively unimportant) fluctuations in T about the local T–S fit. The remaining choice is that of a value for $\Delta\rho$. After some experimentation, we set $\Delta\rho = 0.015$ kg m^{-3}, corresponding to $\Delta S \sim 0.2$. The resulting box size, seen in Fig. 6, provides a reasonable compromise between too much resolution (at which most overturns

are rejected) and too little (at which most are accepted). With fixed resolution, the overturns seen in Fig. 5 were classified as "good" (overturn 1 in Fig. 6a and overturn 4 in Fig. 6b) with the exception of overturn 3 (Fig. 6b), which was classified as "bad" because of the presence of a loop off the local T–S line. Figure 6c illustrates an overturn classified as "borderline"[5] because much of the T–S variability is aligned with the trend of the T–S curve as it exists below the overturn. Many of the borderline classifications come from similar regions where the local T–S curve is changing, often via offsets like that seen here between relatively linear sections. Figure 6d illustrates part of a bad overturn with large T–S variability.

Our calibration dataset used 339 overturns in 47 profiles from NBP409 (including casts in sea states marginal for CTD operations) plus the two available casts taken in open ocean conditions during NBP508, one in the Antarctic Circumpolar Current (with stratification mainly due to salinity) and one in the subtropical gyre (with stratification mainly due to temperature). All overturns were examined, and the water mass variability was classified using the visual inspection scheme with fixed enlargement described above. Diagnostic values computed from the intermediate profile data are plotted in (R_o, ΔN) space in Fig. 7. Visually bad overturns either contain large deviations or loops in the temperature–salinity diagram (large ΔN) or show very unbalanced distributions of Thorpe displacements (small R_o). Good overturns have a tight T–S relationship (small ΔN) and more balanced positive and negative Thorpe displacements (large R_o). Good overturns also tend to lie within the space ($R_o > 0.2$, $\Delta N < 0.003$) shaded in Fig. 7; bad overturns tend to lie outside it, and borderline cases (open circles) are relatively evenly distributed between good and bad regions.

Table 2 summarizes the performance of our two-parameter criteria. The (R_o, ΔN) criterion passes a total of 139 overturns, including 78% (59 of 76) of those visually classified as good, and fails 200 overturns, including 88% (128 of 146) of those visually classified as bad. Only 13% (18 out of the total of 139) of the overturns classified as good are misclassified, that is, classified as good by the two-parameter criterion but bad by visual inspection. Because the borderline classification contains overturns of intermediate character, this category is expected to be distributed approximately equally between the good and bad regions of the (R_o, ΔN) plane; in rough agreement with this expectation,

[5] In the visual classification of overturns, we allow a borderline category for those that are not clearly either very good or very bad.

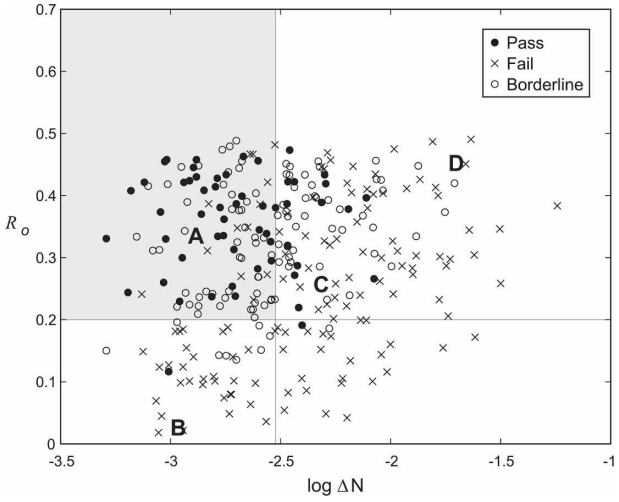

FIG. 7. Performance of the two-parameter diagnostic (R_o, ΔN) on a training set consisting of 339 individual overturns scored visually as good (filled circles), borderline (open circles), and bad (crosses). For clarity, a logarithmic scale is used for ΔN, the range of normal deviation from a locally linear T–S fit. Using the shaded region defined by $R_o > 0.2$ and $\Delta N < 0.003$ (log $\Delta N < -2.52$) for automatic selection of good points, 13% of the values classified as good are misclassified (i.e., should have been classified as bad according to visual scores). Labeled points correspond to those overturns featured in Figs. 4a,b and Figs. 6c,d.

53% of the borderline cases lie within the shaded area of Fig. 7. Table 2 confirms that results from the (R_o, σ_N) criteria are essentially the same; that is, the results do not depend on whether σ_N or ΔN is used to characterize T–S tightness.

In contrast, as seen in Fig. 8 and Table 2, the GK96 requirement of $\xi < 0.5$ for the good criterion failed to make as satisfactory a separation of good from bad. The GK96 criterion passes only 110 overturns, including lower percentages of those visually classified as good (57%) and borderline (26%). In addition, a larger percentage (33%) is misclassified as good when visually scored as bad. This substantial failure rate can be decreased by lowering the acceptance threshold, but this comes at the cost of further increasing rejection of visually acceptable overturns.

TABLE 2. Comparison of the results of the two-parameter criteria suggested here and the ξ criterion of GK96, using a set of 339 individual overturns visually classified as 76 good, 117 borderline, and 146 bad. An error is defined as classification of a visually bad overturn as good. The percent error is the percent of the total number automatically classified as good that were misclassified.

	Pass	Fail	Errors	Percent error
R_o, σ_N	135	204	17	13
R_o, ΔN	139	200	18	13
GK96 ξ	110	229	36	33

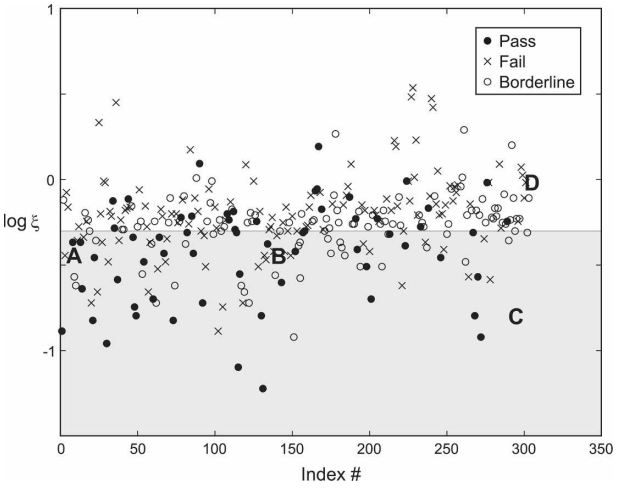

FIG. 8. Performance of GK96's ξ diagnostic plotted vs index number (1–339 within the set) using the same training dataset and visual classification symbols as in Fig. 7. Of the values classified as good by this diagnostic, 33% are misclassified (i.e., should have been classified as bad according to the visual determinations).

Before leaving the discussion of overturn validation, we wish to question whether it is *desirable* to apply a water mass diagnostic (either our ΔN or GK96's ξ) that is based on the assumption that *T*–*S* variability resulting from turbulent mixing should lie along a locally linear *T*–*S* relationship. There are two separate problems with this assumption: the first arises if mixing extends over a range of densities initially characterized by a nonlinear *T*–*S* relationship, and the second comes about through potential consequences of the process of differential diffusion (Gargett 2003).

The first problem is illustrated in Fig. 9, which shows *T*–*S* curves derived from two consecutive CTD downcasts. The first profile (A) contains several small overturns in the upper part of the water column but none below $\sigma_t = 27.82$ kg m^{-3}. In contrast, the subsequent downcast (B) contains two large overturning regions separated by a small but distinct stable region. Both overturns would be discarded by a water mass test; however, we argue that they are more likely real mixing events. First, the density fluctuations in each overturning patch far exceed noise levels and there is no evidence of external contamination of the probes, given the intervening stable region between the two overturning patches and a return to stable conditions below the deeper patch. Second, both overturns encompass density ranges within which the initial *T*–*S* relationship is clearly nonlinear. Careful examination reveals that the salinity range inside each overturn is restricted to the salinity range present in the previous profile for the density range over which the overturn occurs. Because the observed variability of *T*–*S* structure in both overturns is arguably consistent with nonlinear *T*–*S* ranges being mixed within the individual overturning regions, both patches should be interpreted as real overturning regions, of thicknesses 43 and 26 m, respectively. However, both overturns fail our water mass test and that of GK96.

The second problem with assuming that turbulent mixing produces variability only along a local *T*–*S* relationship is the phenomenon of differential diffusion. Accumulating evidence from laboratory and computational studies, together with some provocative ocean observations (Nash and Moum 2002; Merryfield 2002), suggests that differential diapycnal diffusion of *T* and *S* should be expected in the typically weak turbulence resulting from shear instability in the stratified ocean interior. Differential diffusion causes rotation of an initial *T*–*S* line toward horizontal because weak turbulence preferentially mixes away fluctuations in the component with the larger molecular diffusivity (T), leaving a larger fraction of the initial variation in the component with the smaller molecular diffusivity (S). Numerical simulations of differential diffusion reported by Gargett et al. (2003) document the appearance of significant differences between vertical fluxes of the individual scalars over time scales on the order of $(0.1–0.2)T_N$, where $T_N = 2\pi/N$. Because these times scales represent a small fraction of the typical time extent of a shear instability, rotation of the *T*–*S* relationship toward horizontal on the finescale structures within an actively overturning patch may be expected. The finescale regions of flattened *T*–*S* seen in both of the large overturning regions in Fig. 9 are exactly the signatures that would be expected from the action of differential diffusion. While awaiting further clarification of the operation of differential diffusion in the oceanic context, it may be prudent to revise expectations of the degree to which mixing regions should exhibit linear *T*–*S* relationships.

Because the two patches shown in Fig. 9 were the only patches of comparable size observed during the cruise (although not the only ones showing possible evidence of differential diffusion via rotation of finescale features toward horizontal), their rejection via an automated water mass test would have a major effect not only on bulk statistics but also, and perhaps more importantly, on our eventual understanding of the origin of such spatially localized and/or temporally episodic mixing events. Given the problems discussed above as well as the potential importance of large but infrequent events (recalling initial rejection of the signatures of meddies in bottle salinities), we conclude

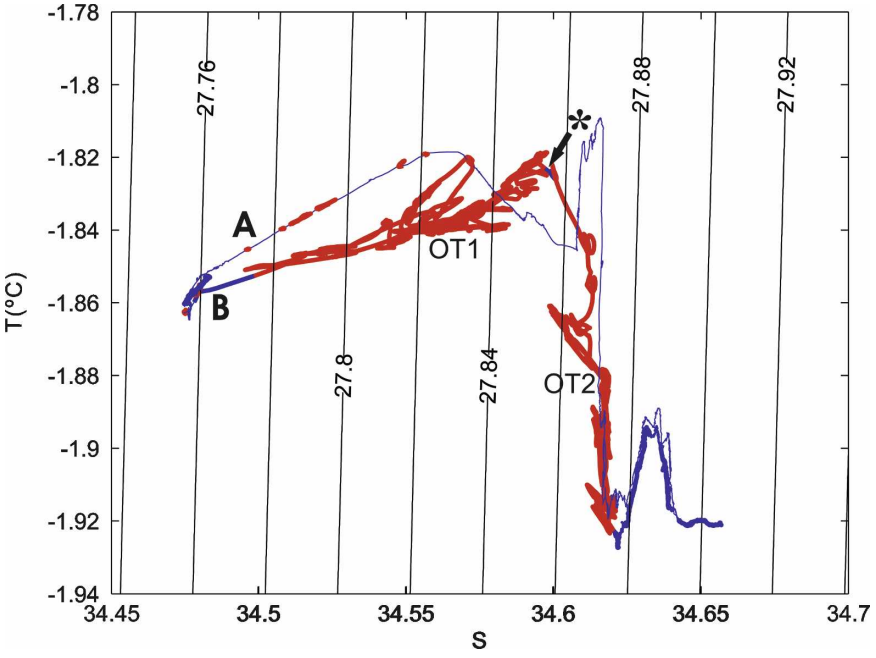

FIG. 9. The T–S curves for two consecutive CTD downcasts with local isopycnals (black lines). Profile A (light blue line, points involved in overturns in red) has no overturns below $\sigma_t \approx 27.6$ kg m^{-3}; the following downcast, profile B (heavy blue line), has two large overturning regions of extents 43 (OT1) and 26 m (OT2), respectively, above and below a small stable density step (at *). Both overturning regions fail water mass tests but are arguably real.

that despite the effort expended here to produce a more reliable water mass criterion, it is more appropriate *not* to apply such a criterion.

5. Discussion and conclusions

Because of the intermittency of shear-generated turbulence in the stratified interior of the ocean, a single profile of Thorpe scales is not particularly useful. However, collections of large numbers of such profiles could provide useful information in two different areas.

First, collections of single profiles distributed spatially would contribute to a basic geography of turbulent mixing in the ocean—the latitude, longitude, and depth parameters of regions where shear turbulence and associated vertical turbulent flux are significant. Such geography is presently rudimentary: in vast volumes of the World Ocean, there are *no* direct measurements of turbulence occurrence and strength. Although Thorpe scales may not provide as accurate a measure of these two properties as do microstructure profiles, even a qualitative measure is better than none. It seems clear that if all deep ocean CTD profiles were routinely processed for Thorpe scales, the ever-increasing database would eventually reveal the geographic dimension of turbulent mixing in the ocean, including definition of mixing "hot spots" associated with topography (Polzin et al. 1996; Naveira Garabato et al. 2004) or latitude (Nagasawa et al. 2002; MacKinnon and Winters 2005). More expensive techniques could then be focused on significant regions to better quantify diapycnal mixing and the processes producing it.

Second, collections of Thorpe scale profiles taken repeatedly with time at a single location would contribute to a description of the temporal variability of shear-generated mixing and thus to identification of its sources. A small-scale illustration of this potential is seen in an example taken from NBP508, where a set of six consecutive Thorpe scale profiles and the acoustic backscatter record from the ship's echo sounder is used to describe the upper ocean mixing environment of interest to MIXURS biologists. In the backscatter record shown in Fig. 10a, depth–time traces of CTD downcasts have been highlighted and numbered. Strong near-surface backscatter (black) seen at the left of the record during cast 1 is clear evidence of ship-induced mixing (carrying air microbubbles of high acoustic cross section) down to 20 m. Although results from the near-surface layer must thus be rejected for this cast, subsequent casts are free of similar ship-induced artifacts. The remainder of the backscatter record reveals undular motion of the base of a surface layer of moderate

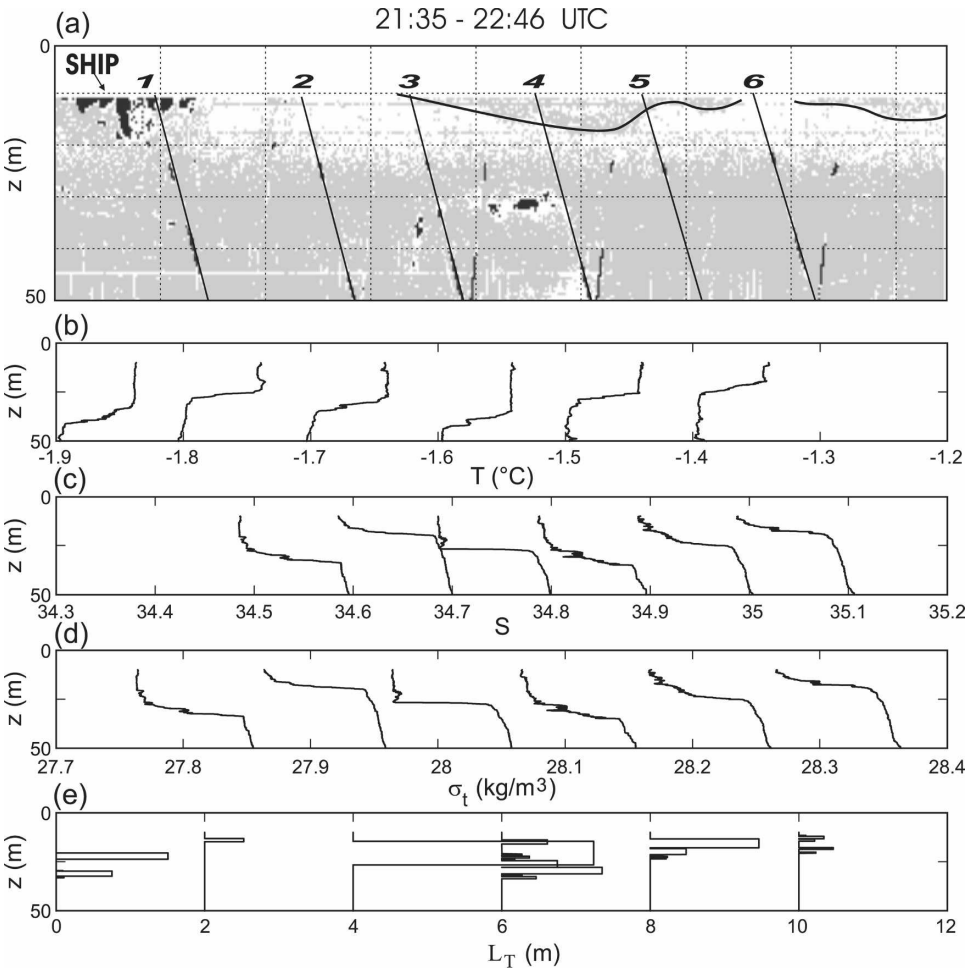

FIG. 10. (a) Time series of relative backscatter from a hull-mounted echo sounder documents contamination from ship positioning (strong surface-origin backscatter at upper left) and depth variation of a surface layer of high relative backscatter. This surface layer is bounded below (line emphasis) by a region of strong gradients, revealed in profiles of (b) T, offset by 0.1°C; (c) S, offset by 0.1; and (d) σ_t, offset by 0.1 kg m^{-3}, from consecutive CTD casts taken at the numbered positions. (e) Profiles of validated Thorpe scales L_T, offset by 2 m, determined from the associated σ_t profiles by the techniques described in this paper.

backscatter (gray) overlying a low backscatter (white) region, a boundary emphasized in Fig. 10a. The CTD casts confirm this picture, revealing the vertical motion of a sharp pycnocline bounding a weakly stratified surface layer. The pycnocline is shallowest in cast 2, deepens to a maximum during cast 4, then shallows again during casts 5 and 6 (during the latter reaching a depth similar to that of cast 2, in agreement with the backscatter record). Thorpe scale profiles provide indications of active mixing associated with the accessible part of the region above the pycnocline, suggesting an actively mixing surface layer with a base that is undergoing significant [O(10 m)] displacements due to internal waves.

The preceding description of the time variability of mixing near the ocean surface depends upon low sea state, but open ocean conditions will normally allow estimates of Thorpe scales only within the stratified interior. This, however, is the very region in which temporal variability of turbulent mixing processes must be regarded as essentially unknown, given the limited time extent of even the longest scientific ocean cruise. If, as presently assumed, shear-driven mixing in the interior is driven predominantly by inertial waves and internal tides, time variability will be a significant factor that must be quantified if we are to produce reliable average values for effects of turbulence. The increasingly frequent deployment of moored profiling CTDs with vertical resolution of tens of centimeters suggests that routine Thorpe scale processing of such data may be the

cheapest way to provide first-order descriptions of the temporal variability of interior mixing.

In summary, this article has outlined methods for calculation of reliable Thorpe scales from density profiles taken with a shipborne CTD lowered at ~30 cm s^{-1}.[6] Although the methods have been developed with shipborne data from an SBE9*plus,* they are easily applied to other CTD models and other deployment techniques. Methods include the removal of questionable instabilities associated with pressure reversals, reduction of the effects of density noise by computation of an intermediate profile before sorting, and overturn verification by a two-parameter (R_o, ΔN) diagnostic. Application of the R_o criterion is highly recommended because it reliably removes overturns that result from a salinity spike at either or both ends of a weakly stratified layer bounded by larger gradients, the most common cause of suspect overturns. In our view, further rejection of overturns based on any measure of *T–S* tightness is not warranted, given expectations of looseness based on the possibility of mixing over regions of nonlinear *T–S* relationship and/or the potential effects of differential diffusion.

Imperfect sensors and ship effects make Thorpe scale calculation from oceanic density profiles a difficult task, exacerbated in the deep ocean by weak density gradients. Some of the procedures involved are less than rigorous, and a review contrasting results of various proposed methodologies over the full range of ocean *T–S* structure would be useful. However, despite imperfections and limitations, a standard processing protocol for Thorpe scales applied uniformly to every CTD profile would quickly begin to reveal patterns of ocean mixing that are worth defining. Widely applied, methods such as those described here could greatly improve our knowledge of shear-generated mixing in the stratified interior of the ocean, using standard shipborne CTD casts to make global-scale maps suggesting major sites of ocean mixing and a new generation of moored profiling CTDs to provide the first reliable information on its temporal variability.

Acknowledgments. We thank the officers and crew of the *Nathaniel B. Palmer* and the technical support staff from Raytheon Polar Services for their help in acquiring the data we have analyzed, and the National Science Foundation Office of Polar Programs for research support under Grant OPP-0125818. We appreciate helpful comments from two anonymous reviewers.

[6] Because of wire time involved, deep CTD stations use a faster lowering rate, which will increase the smallest resolvable vertical overturn. However, it is the geography–time dependence of the largest scale vertical overturns that is of most interest (e.g., because they will dominate diapycnal diffusivity defined via L_T).

REFERENCES

Alford, M. H., and R. Pinkel, 2000: Observations of overturning in the thermocline: The context of ocean mixing. *J. Phys. Oceanogr.,* **30,** 805–832.

Dougherty, J. P., 1961: The anisotropy of turbulence at the meteor level. *J. Atmos. Terr. Phys.,* **21,** 210–213.

Ferron, B., H. Mercier, K. Speer, A. E. Gargett, and K. Polzin, 1998: Mixing in the Romanche Fracture Zone. *J. Phys. Oceanogr.,* **28,** 1929–1945.

Galbraith, P. S., and D. E. Kelley, 1996: Identifying overturns in CTD profiles. *J. Atmos. Oceanic Technol.,* **13,** 688–702.

Gargett, A. E., 2003: Differential diffusion: An oceanographic primer. *Prog. Oceanogr.,* **56,** 559–570.

——, W. J. Merryfield, and G. Holloway, 2003: Direct numerical simulation of differential scalar diffusion in three-dimensional stratified turbulence. *J. Phys. Oceanogr.,* **33,** 1758–1782.

Johnson, H. L., and C. Garrett, 2004: Effects of noise on Thorpe scales and run lengths. *J. Phys. Oceanogr.,* **34,** 2359–2372.

Lueck, R. G., and J. J. Picklo, 1990: Thermal inertia of conductivity cells: observations with a Sea-Bird cell. *J. Atmos. Oceanic Technol.,* **7,** 756–768.

MacKinnon, J. A., and K. Winters, 2005: Subtropical catastrophe: Significant loss of low-mode tidal energy at 28.9°. *Geophys. Res. Lett.,* **32,** L15605, doi:10.1029/2005GL023376.

Merryfield, W. J., 2002: Intrusions in double-diffusively stable Arctic waters: Evidence for differential mixing? *J. Phys. Oceanogr.,* **32,** 1452–1459.

Morison, J. H., R. Andersen, N. Larson, E. D'Asaro, and T. Boyd, 1994: The correction for thermal-lag effects in Sea-Bird CTD data. *J. Atmos. Oceanic Technol.,* **11,** 1151–1164.

Nagasawa, M., T. Hibiya, Y. Niwa, M. Watanabe, Y. Isoda, S. Takagi, and Y. Kamei, 2002: Distribution of fine-scale shear in the deep waters of the North Pacific obtained using expendable current profilers. *J. Geophys. Res.,* **107,** 3221, doi:10.1029/2002JC001376.

Nash, J. D., and J. N. Moum, 2002: Microstructure estimates of turbulent salinity flux and the dissipation spectrum of salinity. *J. Phys. Oceanogr.,* **32,** 2312–2333.

Naveira Garabato, A. C., K. L. Polzin, B. A. King, K. J. Heywood, and M. Visbeck, 2004: Widespread intense turbulent mixing in the Southern Ocean. *Science,* **303,** 210–213.

Piera, J., E. Roget, and J. Catalan, 2002: Turbulent patch identification in microstructure profiles: A method based on wavelet denoising and Thorpe displacement analysis. *J. Atmos. Oceanic Technol.,* **19,** 1390–1402.

Polzin, K. L., K. G. Speer, J. M. Toole, and R. W. Schmitt, 1996: Intense mixing of Antarctic Bottom Water in the equatorial Atlantic Ocean. *Nature,* **380,** 54–57.

Ricker, W. E., 1973: Linear regression in fishery research. *J. Fish. Res. Board Canada,* **30,** 409–434.

Sea-Bird Electronics, cited 2006: SBEDataProcessing_5.37.pdf. [Available online at ftp://ftp.halcyon.com/pub/seabird/OUT-Seasoft-Win32/SBEDataProcessing.]

Stansfield, K., C. Garrett, and R. Dewey, 2001: The probability distribution of the Thorpe displacement within overturns in Juan de Fuca Strait. *J. Phys. Oceanogr.,* **31,** 3421–3434.

Tennekes, H., and J. L. Lumley, 1972: *A First Course in Turbulence*. MIT Press, 300 pp.

Thorpe, S. A., 1977: Turbulence and mixing in a Scottish loch. *Philos. Trans. Roy. Soc. London,* **286,** 125–181.